SYNTHESIS REPORT

FOR PUBLICATION

CONTRACT N° : BRE 2 - CT92 - 0155

PROJECT N° : ~~BRE 2 0155~~ MS 521

TITLE: The Influence of Different Low-Temperature Vapour Deposition Techniques on the Operational Properties of Metastable Hardcoatings

PROJECT COORDINATOR : Lehrstuhl für Theoretische Huttenkunde der RWTH Aachen(LTH)

PARTNERS :
- Lehr -und Forschungsgebiet Werkstoff-wissenschaften, RWTH Aachen (WW)
- Forbairt, Dublin
- Institut National Polytechnique de Grenoble (INPG-LMGP/LTPCM)
- Helsinki University of Technology (HUT)

STARTING DATE: 1.2.1993 DURATION: 36 MONTHS

PROJECT FUNDED BY THE EUROPEAN COMMUNITY UNDER THE BRITE/EURAM PROGRAMME

DATE : 14.6.1996

The Influence of Different Low-Temperature Vapour Deposition Techniques on the Operational Properties of Metastable Hardcoatings

A. von Richthofen, M. Witthaut, R. Cremer, D. Neuschütz
Lehrstuhl für Theoretische Hüttenkunde und Metallurgic der Kernbrennstoffe, RWTH Aachen, Kopernikusstr. 16, 52074 Aachen, Germany

E. Lugscheider, C. Barimani, S. S. Guerreiro
Lehr- und Forschungsgebiet Werkstoffwissenschaften, RWTH Aachen, Jülicher Str. 342-352, 52070 Aachen, Germany

M. Fleming
Materials Technology Department, Forbairt, Glasnevin, Dublin 9, Ireland

R. Madar[1], C. Bernard[2], V. Ghetta[2], C. Jimenez[2], S. Gilles[2]
[1] Laboratoire des Matériaux et du Genie Physique, Institut National Polytechnique de Grenoble, BP 46, 38402 St. Martin d'Hères Cédex
[2] Laboratoire de Thermodynamique et Physico-Chimie Metallurgique, Institut National Polytechnique de Grenoble, BP 75, 38402 St. Martin d'Hères Cédex, France

I. Penttinen, A. Leijala, A. Korhonen
Department of Materials Science and Engineering, Helsinki University of Technology, Vuorimiehentie 2 A, SF-02150 Espoo, Finland

Abstract

Metastable $Ti_{1-x}Al_xN$ films were deposited on HS S substrates by means of MSIP with one compound target, MSIP with two separate targets (graded films), and AIP in a new developed pulsed bias mode to study the influence of different deposition techniques and film compositions on the film properties, their oxidation resistance and mechanical properties. Therefore, films were analyzed in the as-deposited and oxidized state (1 h, 800 'C) with respect to their composition, structure, morphology, binding states of the components, micro- and nanohardness, adhesion , and impact resistance by EPMA, XPS, AES, XRD, HEED, SEM, micro- and nanohardness tests, scratchiest, and impact test. The result was the providing of tailored films with special properties: a high temperature oxidation resistant $Ti_{0.38}Al_{0.62}N$ MSIP film, a $Ti_{0.55}Al_{0.45}N$ AIP film for applications at high mechanical stresses and a $Ti_{0.46}Al_{0.54}N$ film appropriate for a combination of the two stress conditions.

1. Introduction

It was shown that $Ti_{0.5}Al_{0.5}N$ hardcoatings deposited on high speed steel by magnetron sputtering ion plating can give superior performance compared to TiN films under conditions of wear, due to the better high temperature oxidation resistance [4,7]. The reason for this is the formation of a protective layer, highly enriched with Al_2O_3, which prevents rapid oxidation of the nitridic film [5,8,9]. From the technical standpoint it is an interesting question whether the wear resistance can be improved by optimizing the Ti/Al ratio of the nitride MSIP films or by application of another PVD process. Also the deposition of graded films with special properties at the interface to the substrate and at the surface could perhaps lead to better operational properties. Therefore, the influence of the deposition process (MSIP with one compound target, MSIP with two separate targets, AIP in the normal d.c. mode, AIP in the new developed pulsed d.c. mode, and MOCVD) and in case of MSIP films the Ti/Al ratio (targets with ratios of 75/25, 50/50, 40/60, and 25/75 were used) were examined during this Brite-EuRam project. In this work the results of AD? in the d.c. mode are not mentioned because of the very clear improvement of the films by AIP in the pulsed mode. As it was difficult to deposit the metastable films at temperatures lower than 500 "C with MOCVD, the results of the deposited $Ti_{0.85}Al_{0.15}N$ films will be published later. The films were investigated in the as-deposited state and after oxidation at 800 °C (1 h) with respect to composition, structure, binding states of the components, morphology and mechanical properties by means of EPMA, XPS, AES, HEED, XRD, SEM, micro- and nanohardness tests, swatch test, and impact test.

2. Experimental

A. Substrate pretreatment and coating processes

$Ti_{1-x}Al_xN$ coatings of different compositions were deposited by different PVD processes, namely magnetron sputtering ion plating (MSIP) using one compound target, MSIP with two separate targets, and random arc ion plating applying a pulsed bias source.

The substrate material used was heat treated high speed steel type BS-M2 (EN: S 6-5-2). These substrates were automatically polished with diamond paste of 1 pm, ultrasonic cleaned, and inspected before installation in the vacuum chambers.

MSIP deposition with one alloyed Ti-Al target was carried out in a reactive d. c. MSIP system (type Z400, Leybold AG). The Ti/Al ratios of the targets were: 75/25, 50/50, 40/60, 25/75. The 40/60 target was manufactured by mechanical inserting of Al in a Ti plate, the others were powder metallurgical produced. The following deposition parameters were used:
Substrate temperature: 400 "C; bias voltage: -60 V; argon pressure: 1.2 Pa; sputtering power: 400 W; nitrogen reactive gas pressure: 9 % ($p(N_2)/p(N_2)/p(Ar)$).

An MSIP device to allow the co-deposition of Ti and Al in a controlled N_2 atmosphere was

built up. This device enabled the deposition of $Ti_{1-x}Al_xN$ of varying Ti/Al ratios by applying independent power and shutter controls to the individual targets. Sample rotation between the Ti and Al targets via a water cooled specimen holder (rf-biased) enabled atomic mixing and good compositional control during deposition. An optical emission feedback control system was installed in the MSIP chamber, operating by measuring the intensity of a characteristic Ti wavelength within the plasma. This gives a measure of the rate of sputtering of the Ti target. The optimized presented film was deposited with a N_2 reactive gas pressure of 0.5 Pa, an Ar flow of 55 seem, a bias voltage of -70 V and a target current of Ti/Al of 2/0.5 A.

AIP films were deposited in a PVD 20 (Interatom). The arc process has been modified: During heating, a d.c. bias of-1000 V was applied, wheras during deposition a pulsed bias source was used. Powder metallurgical targets (cathodes) composition was 50/50 (Ti/Al ratio). Deposition parameters were as follows: Substrate temperature: 420 "C; duty cycle of pulsed bias: 50%; pulsed d.c. bias voltage: -400 V; pulse frequency: 25 kHz; N_2 reactive gas pressure: 2 Pa; evaporation current applied to cathode: 70.4.

*B. Characterization **of films** by **XPS,** AES, **EPMA, XRD, HEED, SEM,** scratch test, **microhardness** test, impact test, and **nanohardness** test*

$Ti_{1-x}Al_xN$ films were tested in the as-deposited and oxidized state with respect to composition, binding states, crystallographic structure, morphology, and several mechanical properties like adhesion, micro- and nanohardness, and impact resistance.

The composition of the hard coatings was determined by a thin film EPMA technique according to [1] based on Monte Carlo Simulation. This was chosen to differentiate between the oxygen fraction incorporated in the coating and a contribution from a thin oxide layer at the surface. For this analysis the electron energies 2.5, 5.0 and 10 keV were applied. The measurements were carried out with a Camebax SX50 microprobe analyser equipped with four wavelength dispersive spectrometers. The X-ray signals were calibrated on the following standards: pure freshly polished aluminium for Al Kα, TiN or Fe_4N for N Kα, Ti or TiN for Ti Lα, and an electrically conductive $BaFe_{12}O_{19}$ for O Kα. The Ti Ll overlap with N Kα was corrected by a procedure, in which the overlapped Ti Ll-signal is recalculated from a measurement on a Ti-standard as pure Ti or TiC and subtracted from the sum signal measured on the unknown sample. Matrix effects are considered in this correction.

Auger -' and photoelectron spectra were taken of sputter-cleaned films (5 keV Ar^+; 70° surface normal to beam; 50 nA; 10 rnin) using a Cameca Nanoscan 50 microprobe with XPS attachment, operating with a 5 keV electron-beam (currents: in the range of 2-40 nA; scanned area: 5 mm^2) and non-monochromized Al Kα X-rays (200 W) respectively. Using a semidispersive energy analyzer (MAC3) in the pulse counting mode (direct mode) with constant energy resolution, X-ray photoelectron spectra were recorded in the range of O-636 eV binding energy; energy resolution: 1 eV; step: 0.2 eV; dwell time: 20 ms; cycles: 50, and Auger electron spec-

tra were acquired in the multi window mode; energy resolution: 1 eV; step: 0.5 eV; dwell time: 5 ms; cycles: 1000. Energy calibration of the analyzer was carried out on sputter cleaned Ag and Au, using the Ag-$M_4N_{45}N_{45}$ line (357.9 eV) and Au-$M_5N_{67}N_{67}$ line (201 5.7 eV). XPS and AES peak shifts due to charging effects were corrected at the $Ar2p_{3/2}$ line (242.25 eV binding energy) or Ar-$L_3M_{23}M_{23}$ (maximum $^1D/^3P$: 211.1 eV kinetic energy) used as internal standard. It is assumed that the Auger- and photoelectron line energy of the sputter-implanted Ar is independent of the chemical environments associated with Ti-Al-N films of different compositions.

For quantative evaluation of the films by XPS the Al2p, Ti2p, N1s, and O 1s peaks were considered. The background was subtracted according to the method of Shirley and the relative sensitivity factors for Al, Ti, O, and N were determined using sputter-cleaned γ-Al_2O_3 and TiN as standard.

The chemical binding states of the components were investigated by analyzing the N-KU and O-KLL Auger spectrum as well as the Auger Al-$KL_{23}L_{23}$ (1D) peak and Ti-LMM spectrum and Al2s, Ti2p, N1s, and O 1s photoelectron peaks.

XRD analyses were made on a Siemens D500 goniometer with thin film attachment at an X-ray incident angle of 3° to the surface. The scanned angular range was 20 °<26<700. Cu-Kα radiation (O. 1542 nm) was used; X-ray power was 900 W.

HEED analysis was carried out using a 35 keV electron beam at an incident angle of less than 1“ to the surface. The diffraction pattern was displayed via a fluorescent screen and recorded with a Hi8-video camera (SONY). All patterns were digitalized; image processing and analysis were carried out by a computer. The experimental setup is described in detail by [2].

SEM micrographs were taken by either a DSM 962 (Zeiss) or a Joel 8600 "Superprobe".

Scratch tests were performed on a LSRH-Revetest (SCEM). Microhardness (HV0.05) was determined by a Micromet-Buehler, nanohardness by using Nanotest 550 Nanohardness Tester at an initial load of 50 μN. The impact tester was self constructed.

C. ***Oxidation treatment***

Oxidation of the $Ti_{1-x}Al_xN$ films was carried out in a high temperature tube furnace (Hartung). The oxidation conditions were: artificial air with $p(N_2)$ = 0.79 bar and $p(O_2)$ = 0.21 bar; oxidation time 1 h; oxidation temperature 800 ‘C.

3. Results and discussion

3.1 Coatings in the as-deposited state

A. Composition of the $Ti_{1-x}Al_xN$ films

The bulk composition of the $Ti_{1-x}Al_xN$ films was determined by thin film EPMA. The analysis of the films given in table 1 shows that, neglecting the insignificant oxygen content, compounds are formed with a metal to nitrogen ratio of virtually one. One can conclude the following film compositions: $Ti_{0.74}Al_{0.26}N$, $Ti_{0.46}Al_{0.54}N$, $Ti_{0.38}Al_{0.62}N$, and $Ti_{0.25}Al_{0.75}N$ in case of the MSD? films, and $Ti_{0.55}Al_{0.55}N$ of the AIP film (nevertheless these films will be often labeled in this report corresponding to the target composition 75/25, 50/50, 40/60, and 25/75, respectively). The Ar content lies in the region of the detectable limit of the microprobe at 0.5 at-%. An analysis of the MSIP film deposited with two separate targets cannot be given as it is graded, starting with' Ti at the interface to the substrate, followed by an increase of nitrogen and then aluminum up to a film composition of about $Ti_{0.5}Al_{0.5}N$ at the surface.

Compared with the Ti/Al ratio of the targets, the Al content of the 75/25, 50/50, and 40/60 MSIP films is slightly higher than expected. By contrast, the ratio of the Al rich 25/75 film is almost exactly that of the target. In contrast to that, the Ti/Al ratio of the arc film is higher than that of the target. Here has to be mentioned that this ratio is strongly influenced by the duty cycle, as shown in figure 1.

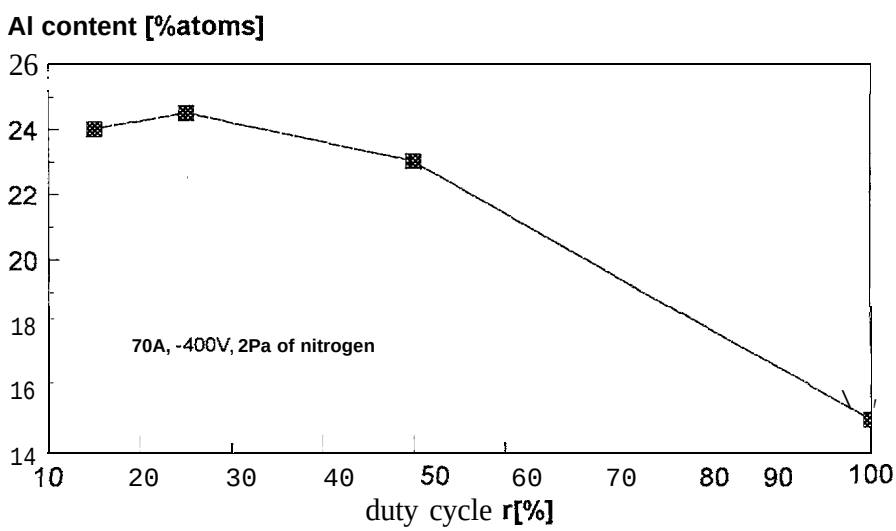

Figure 1: Aluminum content of AIP $Ti_{1-x}Al_xN$ films as function of the time the bias is on

Evaluation of the measured photoelectron spectra of the MSIP films deposited by using powder metallurgical targets with regard to the chemical composition of the surface near region is also included in table 1, showing that the Ti/Al ratio corresponds almost to the bulk ratio, whereas the oxygen content is considerably higher.

Deposition process	Expected atomic Ti/Al ratio	film composition in at-%							
		EPMA (bulk)				XPS (surface)			
		Ti	A I	N	o	Ti	A I	N	o
MSIP	75/25	36.2	13.1	50.4	0.3	37.1	13.6	41.6	7.7
MSIP	50/50	20.8	24.7	51.5	3.0	23.2	26.8	33.9	16.1
MSIP	40/60	17.7	29.2	49.9	3.2	n.a.	n. a.	n.a.	n.a.
MSIP	25/75	12.4	37.2	50.3	0.1	13.4	35.7	40.6	10.3
AIP	50/50	25.3	20.3	52.3	2.1	n.a.	n.a.	n.a.	n.a.

Table 1: Bulk and surface composition of as-deposited MSIP and AIP films deposited with one compound target

B. Chemical binding states of the components of the films

The AES analyses of the chemical binding states of the components of the $Ti_{0.74}Al_{0.26}N$, $Ti_{0.46}Al_{0.54}N$, and $Ti_{0.25}Al_{0.75}N$ film are represented in figures 2 a and b. The Al-$KL_{23}L_{23}(^1D)$ line and also the Ti-LMM and N-KLL spectra of the films were obtained in the multi-window mode. For comparison, the $KL_{23}L_{23}(^1D)$ line of aluminium in the metallic, nitridic (AlN), and oxidic (γ-Al_2O_3) binding state were examined, together with spectra of titanium in metallic and nitridic (TiN) bond. The chemical shift of the Al-$KL_{23}L_{23}(^1D)$ line indicates that the binding state of Al in the Ti rich 75/25 and 50/50 layer differs significantly from that of the Al rich 25/75 layer. The shift of the Al-$KL_{23}L_{23}(^1D)$ line of the Ti rich layers is 2.7 eV or 2.8 V, but that of the Al rich 3.6 eV, related to metallic aluminium. The comparison with nitride bonded aluminium (in hexagonal AlN) shows that the covalent nature of the bond in aluminium rich $Ti_{0.25}Al_{0.75}N$ is more pronounced than in the case of the more titanium rich nitride.

The spectrum of the metal shown in figure 2 b represents the Auger lines of the Ti-LMM series, the lines in the spectra of the nitrides correspond to a superposition of the Ti-LMM series and the N-KLL series taken from $Ti_{1-x}Al_xN$.

Due to the overlapping of the N-KLL peaks with the Ti-$L_3M_{23}M_{23}$ peaks and due to the influence of the Ti-N bond on the shape of the Ti-$L_3M_{23}V$ peak, clear differences can be seen between the Ti-LMM Auger spectrum of the alloys and the spectrum of metallic titanium. The highly resolved spectra of $Ti_{1-x}Al_xN$ layers show that the Ti-$L_3M_{23}V$ Auger line of nitridic Ti is split up into two lines, separated by ca. 4 eV. The position of the split peak is, within the

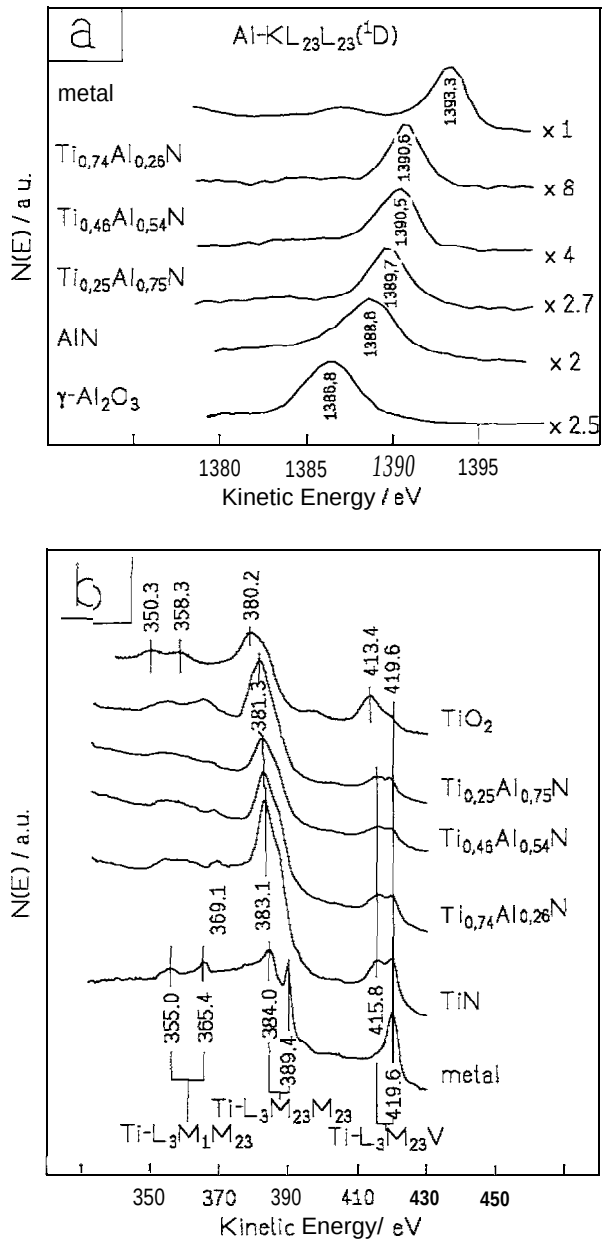

***Figure* 2:** *Auger electron spectra taken in the direct mode; a: Al and b: Ti in different binding states*

limits of accuracy of measurement, independent of the Ti/Al ratio of the Ti-Al-N alloy. The Ti-$L_3M_{23}M_{23}$ peak at 389.4 eV is only faintly recognizable as a narrow shoulder in the alloy spectra. The peak maximum of the Ti-$L_3M_{23}M_{23}$ lines superposed by the N-KLL lines shifts with increasing Al:Ti ratio from 383.1 in the case of TiN to 381.3 eV ($Ti_{0.25}Al_{0.75}N$). position and fOrm of the $L_3M_1M_{23}$ transitions of metallic titanium and the hexagonal alloy are similar and differ significantly from those of the cubic alloys. This indicates a change in bonding character of titanium from the hexagonal to the cubic nitride structure.

C. *Structure*

The structure and texture of the $Ti_{0.74}Al_{0.26}N$, $Ti_{0.46}Al_{0.54}N$, and $Ti_{0.25}Al_{0.75}N$ MSIP film *were* determined by means of High Energy Electron Diffraction (HEED).

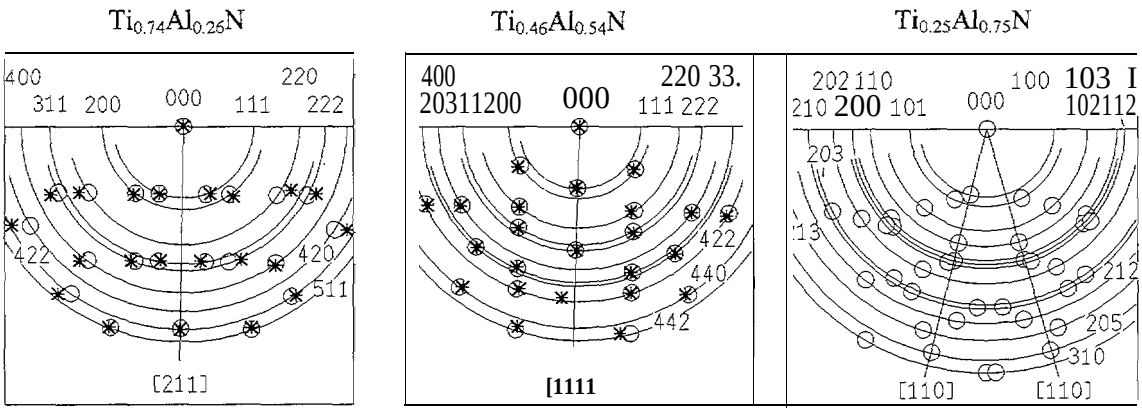

Figure 3: Evaluated HEED patterns of MSIP films; positions of maxima of intensity of arcs and corresponding computed patterns for the determined structures and textures

From the HEED patterns the pictures shown in figure 3 a-c were constructed, where the small crosses represent the observed intensity maxima and the rings the calculated maxima for the detected textured structure (crosses are omitted in case of the 25/75 film for better survey; the correspondence is comparable to that of the other films). The 75/25 film is grown in a cubic B 1 structure with a [211] texture and a lattice parameter of 4.21+0.05 Å. This texture corresponds to a [1 11] texture, whose orientation axis is inclined at 19.47° to the substrate normal. The 50/50 film shows likewise a cubic B 1 structure, grown with [1 11] texture, but with the orientation axis parallel to the substrate normal. Its lattice parameter was determined as 4.16+0.05& The 25/75 film has a hexagonal B4 structure with a [11 O] texture. Two orientation axes can be seen, the one inclined -15°, the other+15° to the substrate. normal. Its lattice constants are a_0 = 3.21+-0.04 Å and c_0 = 5 .04±0.06 Å. The relative inaccuracy of the evaluated lattice constants is a consequence of the lack of precision involved in determing the camera length with grazing incidence of the electron beam.

To examine the structure of the bulk of the films and to determine the lattice parameters more exactly, diffraction patterns of the films were taken by means of thin film XRD.
The diffraction patterns of the $Ti_{0.74}Al_{0.26}N$, $Ti_{0.46}Al_{0.54}N$, and $Ti_{0.25}Al_{0.75}N$ MSIP films are represented in figure 4. The evaluation reaveled that the crystal structure of the near surface region corresponds to that of the bulk. The lattice constants for each line were determined individually, the recorded a_0 corresponding to the mean value. The scatter indicates that the films did not grow in ideal cubic or hexagonal structure.

A comparison of the lattice constants of the cubic $Ti_{1-x}Al_xN$ films with that of cubic TiN (JCPDS-file no: 38-1420 [3]) shows that with increasing Al-content of the cubic films the lattice constants diminish. The reason for this is that, according to [4], the Ti-atoms in the TiN

lattice are substituted with Al-atoms of smaller radius, so that the equilibrium spacings are reduced. A converse effect can be observed with the $Ti_{0.25}Al_{0.75}N$ film, where the M-atoms in the hexagonal AIN are substituted with Ti-atoms. The lattice constants a_0 and c_0 are distinctly greater than that of hexagonal AlN (JCPDS-file no: 25-1133 [3]).

The value of the lattice constant of $Ti_{0.74}Al_{0.26}N$ is lower by 0.01 Å and of $Ti_{0.46}Al_{0.54}N$ lower by 0.03 Å than the values determined by Ikeda et al. [5] for layers of virtually similar composition. However, these were determined for films deposited at -100 V bias. Håkansoon et al. [6] report that the lattice constant of the 50/50 layer increases markedly with rising bias in the range -80 to -150 V. A possible reason could be that the bias produces internal stresses in the layers, which would explain the lower lattice constants found at -60 V in the deposited layers in the present work. Measurements carried out here indicate that the effect of bias on the lattice constants becomes more pronounced with rising Al-content of the cubic films. To verify this observation, a TiN film was deposited at a bias of-60 V. The lattice constant of this layer at 4,252 Å was only 0.008 Å less than the a_0 value of TiN as determined by Ikeda et al. [5]. This result supports the assumption that the effect of bias diminishes with decreasing AI-content of the cubic $Ti_{1-x}Al_xN$ layer.

For further optimization of the MSIP films the Al content should be increased near to the phase transformation point between cubic and hexagonal structure, which is not exactly known, but the film had to be still in a cubic structure. As shown in figure 5, this could be reached by the deposition of the $Ti_{0.38}Al_{0.62}N$ film. The layer has grown in the cubic B 1 structure with a lattice constant of 4.143 ± 0.005 Å, that means the same tendency described above.

The crystallographic structure of the $Ti_{0.55}Al_{0.45}N$ AIP-P film (50 % duty cycle) was determined as cubic B **1** structure with a lattice parameter of 4.200 ± 0.016 Å. According to the higher Ti/Al ratio as compared with the $Ti_{0.46}Al_{0.54}N$ MSIP film the lattice constant is 0.046 Å lower.

D. Morphology

The SEM micrographs, figure 6, show the surface of the cross-sectional fracture of the MSIP films deposited with one compound target. Columnar growth of the crystallite can be seen in case of the cubic films. The diameter of the columns, as measured near the surface, decreases with increasing Al:Ti ratio of the films, the layers becoming more compact. Columnar growth

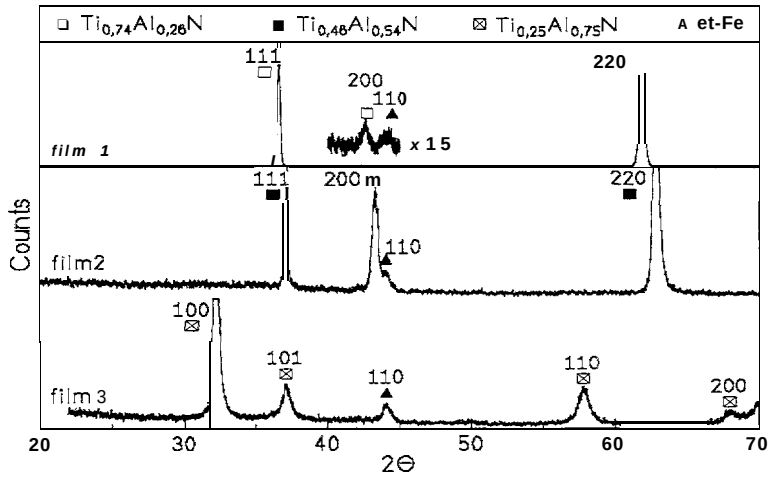

$Ti_{0.74}Al_{0.26}N$	B1	a_0:	4.214 ± 0.002 Å
$Ti_{0.46}Al_{0.54}N$	B1	a_0:	4.154 ± 0.008 Å
$Ti_{0.25}Al_{0.75}N$	B 4	a_0:	3.17 ± 0.002A
		c_0:	5.014 ± 0.01 Å

Figure 4: Crystallographic structure of the bulk of MSIP films

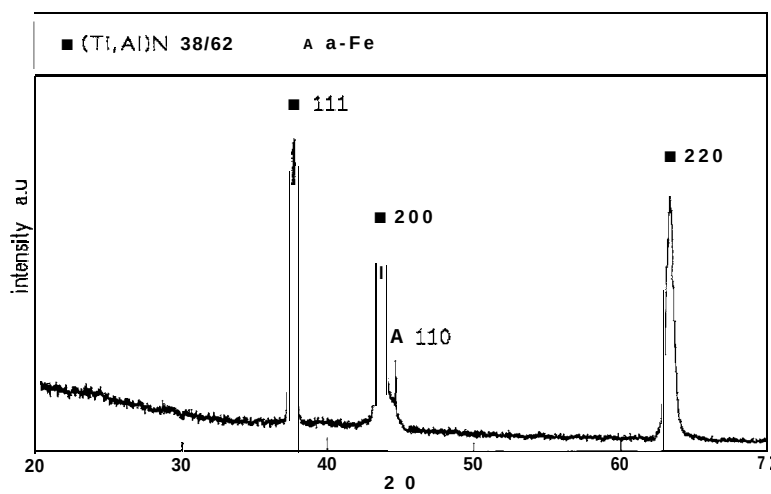

$Ti_{0.38}Al_{0.62}N$ **MSIP B1** a_0: 4.143+ 0.005A

Figure 5: *Crystallographic structure of the bulk of the* 40/60 *MSIP film*

cannot be observed in the hexagonal -film, the layer, by contrast, appearing to have grown as a fine crystalline structure.

The thickness of the films determined from SEM micrographs is 3.8 μm in case of $Ti_{0.74}Al_{0.26}N$, 3.7 μm of $Ti_{0.46}Al_{0.54}N$, 4.1 μm of $Ti_{0.38}Al_{0.62}N$, and 4.9 μm of $Ti_{0.25}Al_{0.75}N$. Each of the four films was deposited using a de-power of 400 W. It was expected that the film thickness would increase with increasing Al: Ti ratio of the compound target, because the sputter rate increases with increasing Al content of the target. The $Ti_{0.46}Al_{0.54}N$ film, however, shows a lower

thickness than all others, This indicates that it has grown in a denser structure, which is very important for high oxidation resistance.

As visible from the SEM micrograph of the cross-sectional fracture (figure 7), the 50/50 MSIP deposited with two separate targets is grown in a dense, columnar structure without any defects. Morphology and thickness of the film are comparable to the films deposited with an alloyed target,

Figure 7 also shows the cross-sectional fracture of the AIP coating. The film has grown in a dense, columnar structure, This morphology is comparable to that of AIP films deposited for comparison in the d.c. mode without pulsed bias. But the pulsed deposited film, primarily in the as-deposited state, shows superior adhesion to that of the d.c. produced. The droplet density in both films, deposited in the d.c. and the pulsed mode, is similar, with the average defect size markedly larger in case of the pulsed one.

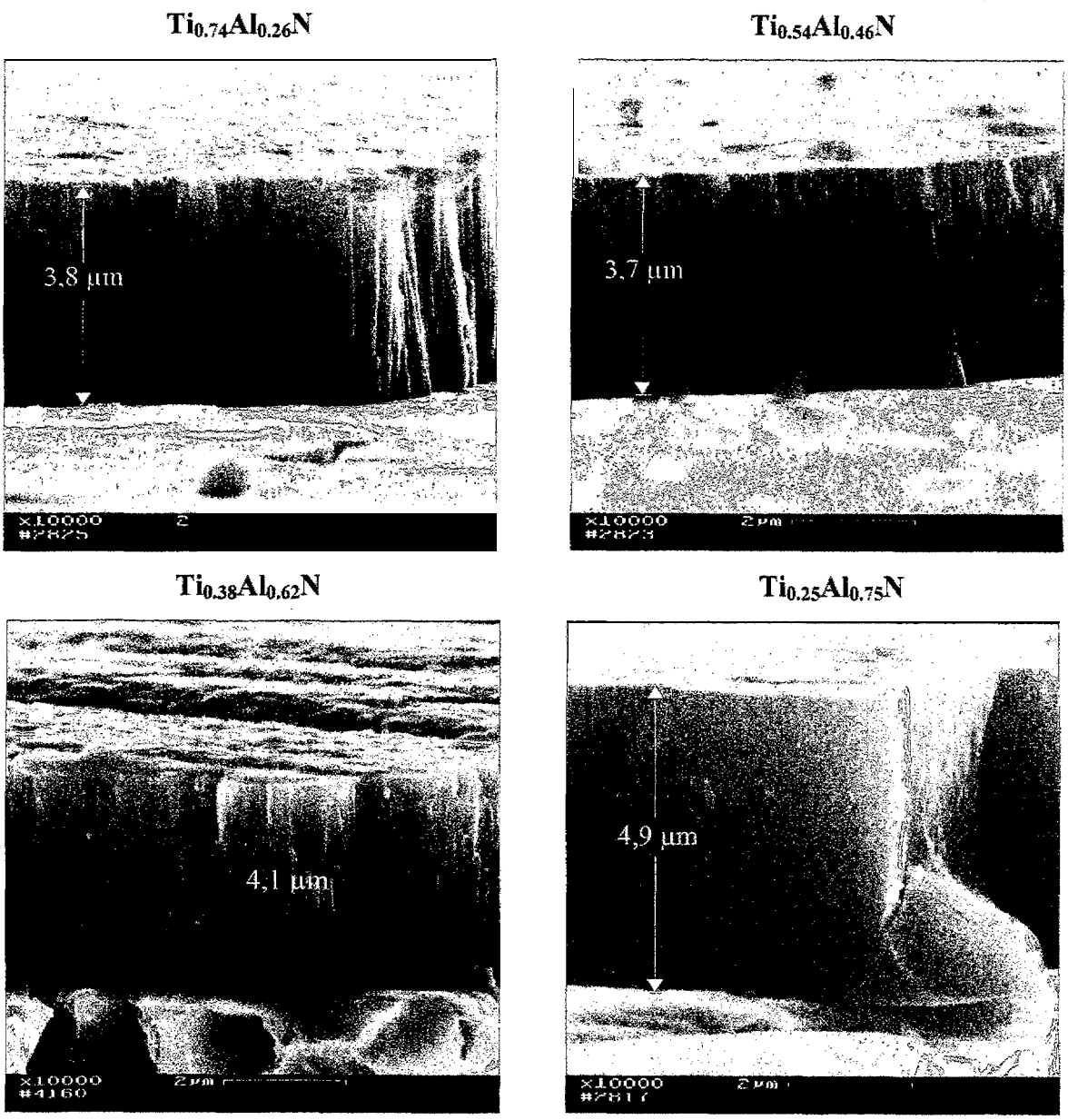

Figure 6: *SEM micrograph of the cross-sectional fracture of MSIP films*

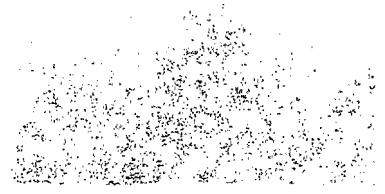

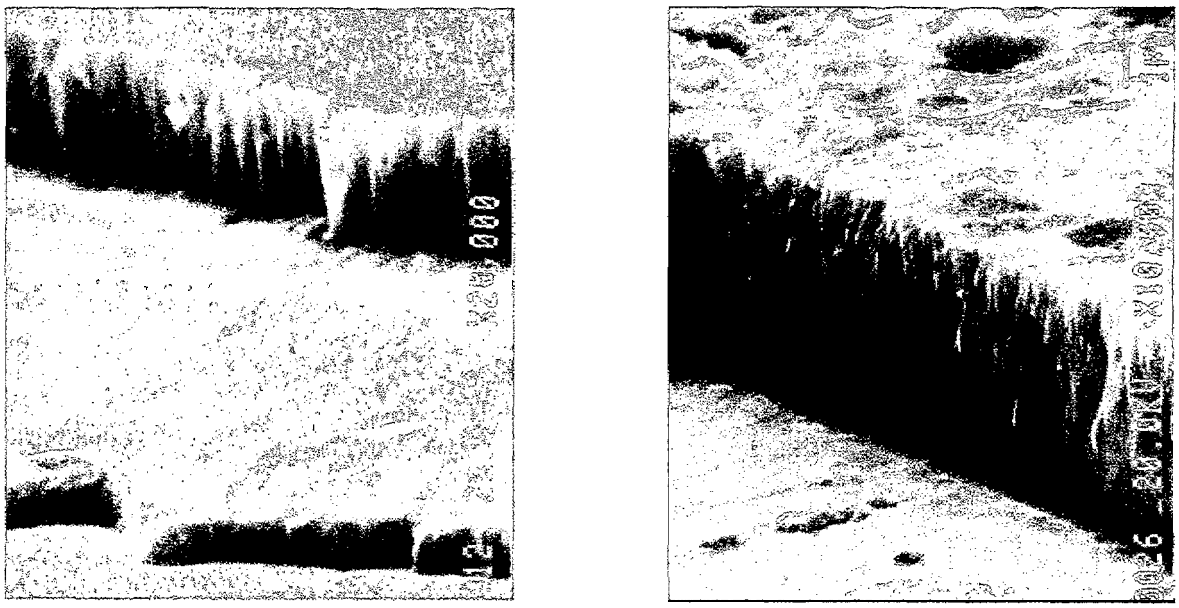

Figure 7: *SEM micrograph of the optimized $Ti_{0.5}Al_{0.5}N$ MSIP film deposited with two separate targets (left) and of the AIP film (right)*

E. Mechanical properties

film	microhardness HV0.05		Adhesion Lc [N]		nanohardness at 450 nm [GPa]	
	as-deposited	oxidized	as-deposited	oxidized	as-deposited	oxidized
$Ti_{0.74}Al_{0.26}N$ MSIP	1550	n.a.	45	n.a.	n.a.	n.a.
$Ti_{0.46}Al_{0.54}N$ MSIP	1600	2900	45	70	n.a.	n.a.
$Ti_{0.38}Al_{0.62}N$ MSIP	2190	687	35	35	20	17
$Ti_{0.25}Al_{0.75}N$ MSIP	3000	2350	32	20	n.a.	n.a.
$Ti_{0.5}Al_{0.5}N$ MSIP (dual target)	1200	ma.	28	n.a.	20	13
$Ti_{0.55}Al_{0.45}N$ AIP	2240	1425	60	30	<10	30

Table 2: *Mechanical properties of the $Ti_{1-x}Al_xN$ films*

Some results of mechanical testing can be seen from table 2. For comparison (see below) values of the films oxidized 1 hat 800 “C are already included.

The microhardness of homogeneous MSIP films increases with increasing Al content. The graded MSIP film is not as hard as the comparable $Ti_{0.46}Al_{0.54}N$ coating. As already known from arc coatings deposited in the normal d.c. mode, this deposition process leads to very hard films, values of nearly one order of magnitude higher than those of MSIP films of the same composition can be achieved.

Adhesion, expressed by the critical load, shows a contrary tendency, decreasing values with increasing Al content are observed. The graded film shows a slight lower value. A higher ad-

hesion as compared to the MSIP films is found for the AIP films, as a consequence of the metal ion bombardment before deposition, during the heating phase in the d. c. mode.

In selected cases, nanohardness was measured showing equal values for the MSIP films and, surprisingly, a lower one in case of the AIP film. It has to be mentioned that the nanoindentation response of the AIP coatings displayed considerable scatter. This is likely a consequence of the lack of surface smoothness due to the presence of droplets and pin holes formed during deposition

3.2 ***Coatings in the oxidized state***

A. Determination of the oxidic scales by XPS, EPMA, and AES

The oxidic scales of the MSIP films deposited with one compound target and of the AIP film were determined after oxidation at 800 "C (1 h) by EPMA and, in selected cases, by AES and XPS.

A crater which ranges into the non oxidized region of the nitridic coating was sputtered by an Ar^+ ion gun. With high resolution AES multpoint analysis carried out at the edge of the crater the chemical binding states of the components with depth were determined in case of the $Ti_{0.74}Al_{0.26}N$, $Ti_{0.46}Al_{0.54}N$, and $Ti_{0.25}Al_{0.75}N$ film. The integral composition of the surface of the oxide layers was determined by XPS. Along the crater edge an EPMA linescan analysis was performed. The shape of the crater was measured by microprofilometry in case of the above mentioned films. The EPMA linescan profile was then convoluted with the crater profile to a real composition depth profile. In case of the $Ti_{0.38}Al_{0.62}N$ MSIP and the $Ti_{0.55}Al_{0.45}N$ AIP films an EPMA linescan analysis under the same conditions was carried out, presented with the distance parallel to the surface as x-axis. In case of the $Ti_{0.38}Al_{0.62}N$ MSIP coating from the differences of the integral EPMA analysis in different depths a depth profile with the mass coverage as depth scale was calculated. This reconstruction technique, also used for the other MSIP films for comparison, allows an estimation of the thickness of the oxide layer without measuring the crater shape.

Table 3 shows the quantification of the XPS analysis of the major components Al and O and the minor components Ti and N at the surface of the oxidic overlayers.

film	Al [at-%]	Ti [at-%]	O [at-%]	N [at-%]
$Ti_{0.74}Al_{0.26}N$	37	2	60	1
$Ti_{0.46}Al_{0.54}N$	38	2	59	1
$Ti_{0.25}Al_{0.75}N$	34	4	61	1

***Table 3: XPS** analysis results of the surface of the oxide layer formed after oxidation at 800 °C on MSIP films*

Figure 8 shows the composition of the oxide layers formed on these MSIP films with depth, determined by EPMA. Evaluation of the profiles indicates that generally the oxide overlayer consist of two sublayers which differ significantly in the Al and Ti content, respectively. The surface near sublayer I is mainly composed of Al and O in a ratio of 2:3. The Ti content at the surface is generally about 3 at-%. As opposed to this, the Ti/Al ratio of sublayer II seems to depend on the Ti/Al ratio of the nitridic bulk. With increasing Al content of the nitridic film the Al content of the sublayer II increases. The nitrogen content at the surface is less than 1 at-% in case of all oxide layers. In the oxide layer of the Ti rich and the 50/50 film the nitrogen content increases continuously from the surface in direction to the nitridic bulk, whereas in case of the Al rich film the nitrogen increases not down to the interface between sublayer D./nitride film (III). The course of the depth profiles indicates wide interfaces between the sublayers, caused by their microscopical interlocking. The oxide overlayer formed on the $Ti_{0.46}Al_{0.54}N$ has, with about 250 nrn, half the thickness of the other two.

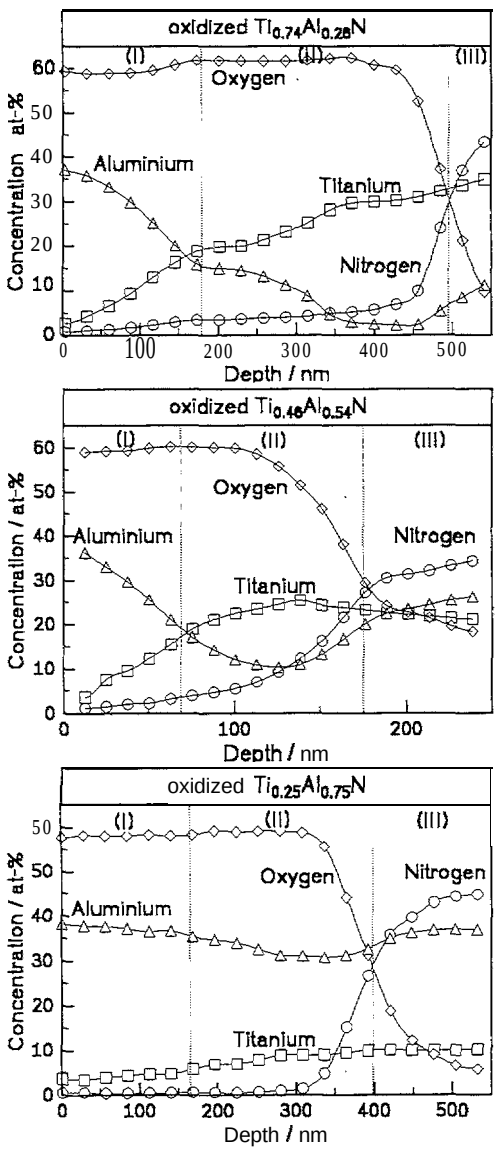

Figure 8: EPMA crater edge linescan profiles with depth of the oxide overlayers of MSIP films

The later developed cubic $Ti_{0.38}Al_{0.62}N$ MSIP film was analyzed by EPMA after oxidation at 800 °C, too. Figure 9 shows the depth profile of the oxide layer. There are visible distinct differences in the build-up of this oxidic overlayer in comparison to the other three. The main part of the oxide layer seems to be composed of Al and O in the ratio of 2:3, i.e. probably alumina with a very low Ti content. The Ti and N content increases continuously in direction to the bulk and no division into two sublayers is detectable. Measuring with different primary electron energies and applying a reconstruction technique it was possible to prove that the surface near half of the oxide layer contains less than about 1 at-% N and Ti. The thickness of the oxide layer, in terms of mass coverage, is about 20-25 $\mu g/cm^2$. For comparison, the same method applied to the $Ti_{0.46}Al_{0.54}N$ film has shown about 80 $\mu g/cm^2$, i.e. the oxide overlayer formed on the 40/60 film has a thickness of about 70-80 nrn. Concerning the oxidation resistance this means the best result of all investigated films.

Generally, the build-up of the oxide overlayer formed on the $Ti_{0.55}Al_{0.45}N$ AIP film is comparable to that of the 50/50 MSIP coating (figure 10). The visible inhomogenities in the composition especially at the

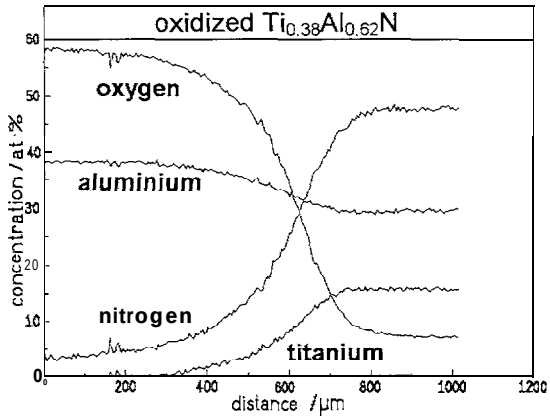

***Figure** 9: EPMA crater edge linescan profile of the oxide overlayer of the $Ti_{0.38}Al_{0.62}N$ MSIP film*

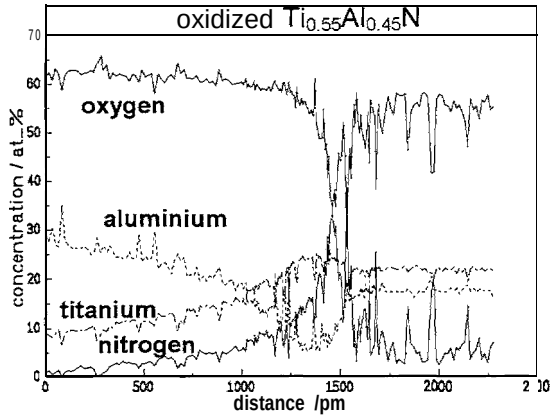

***Figure 10:** EPMA crater edge linescan profile of the oxide overlayer of the $Ti_{0.55}Al_{0.45}N$ AIP film*

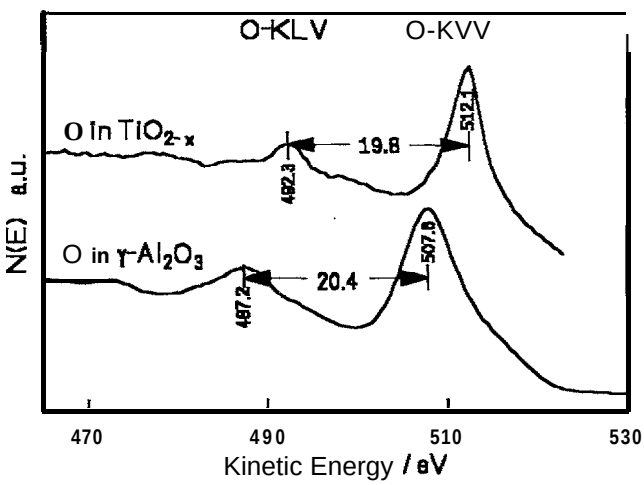

***Figure 11:** AES reference spectra of oxygen in TiO_{2-x} and Al_2O_3*

interface to arid in the nitride coating are probably caused by cylindrical formations of these arc coatings which were observed by SEM (see below). From the EPMA analysis they seem to be oxides, at least in the nitridic bulk.

In order to determine the chemical binding states of the components with depth, high resolution AES multi point analyses at the crater edge were performed. For identification of the binding states, additionally to the reference spectra represented in figure 2, the reference spectra of oxygen in TiO_{2-x} and γ-Al_2O_3 were taken (figure 11). The spectrum of O in these two phases differs significantly in the energy of the O-KVV line and the relative distance between the KVV and the KL_1V peak. The stoichiometry of the reference sample in the bulk is, determined by EPMA, TiO_2.

Figure 12 shows as an example the AES spectra of Ti, Al, O, and N taken along the crater edge of the oxide layers of the 50/50 and the 25/75 MSIP films. The spectra are taken at the surface (I), at the interface region between sublayer I and H detected by EPMA (II), from sublayer II (III), at the interface between sublayer II and the nitridic film (IV), and at the crater bottom (V), i.e. the nitridic bulk.

Evacuation of the Al-$KL_{23}L_{23}(^1D)$ peak position regarding the binding state of aluminum shows

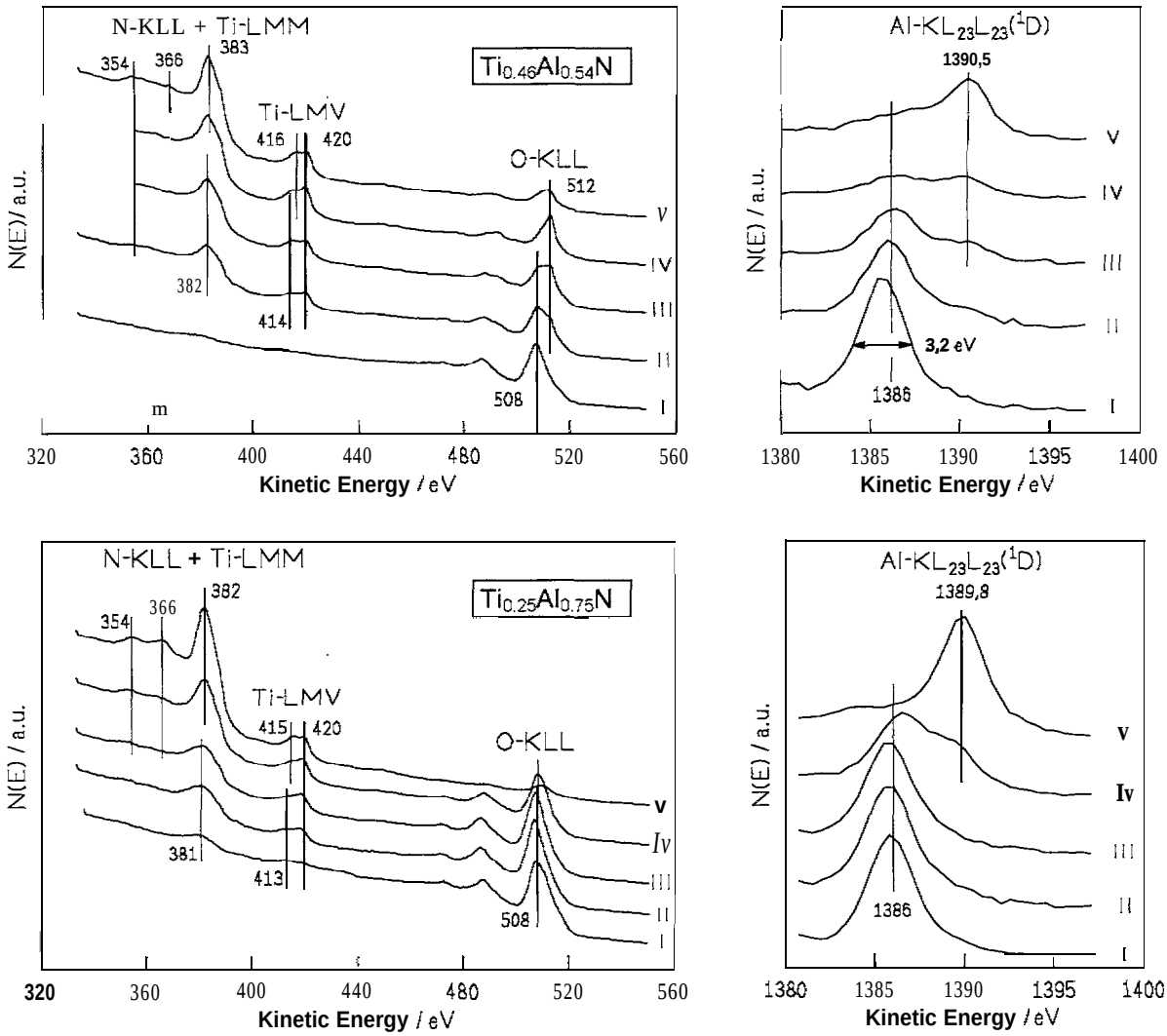

Figure 12: *AES spectra of Ti, Al, O, and N in different depths of the oxide layer on the 50/50 and the 25/75 film; taken along the crater edge, starting from the surface (I) to the crater bottom (V)*

in consideration of the reference spectra (figure *2)* that Al at the surface and in sublayer I is oxidic bonded probably as γ-Al_2O_3, whereas in sublayer 11 it is present as Al_2O_3 and nitridic bonded $Ti_{1-x}Al_xN$. Here the nitridic bonded portion is smaller. At the crater bottom Al mainly occurs in nitridic bonding.

Analysis of the O-KLL group confirms the tendency of the existence of oxidic bonded Al in dependence of the depth of the overlayer. Oxygen is present in two binding states in the oxidic overlayers: as $A1_20_3$ and bonded to Ti as TiO_{2-x}. This is visible very clearly in case of the *50/50* film, wheras in case of the *25/75* film one can recognize O bonded to Ti just from the faint shoulder of the O_{Al}-peak. This is caused by the smaller Ti content of sublayer II of the *25/75* film (about 10 at-%) as compared to the 50/50 film (about 20 at-%). At the surface of the oxidic overlayers oxygen is mainly bonded to Al, with increasing depth the portion bonded to Ti increases. A comparison of the O content bonded to Al and to Ti in sublayer II shows that with increasing Al content of the nitridic $Ti_{1-x}Al_xN$ film the O_{Al}/O_{Ti} ratio increases. At the crater

bottom O is mainly bonded to Ti. Evaluation of shape and position of the (.)-peaks of the O-KII group does not indicate any O-N bonding or that oxygen is bonded in a homogeneous Ti-O-N or AI-O-N phase.

Evaluation of the N-KLL and Ti-LMM spectra, which partially overlap each other, confirm the detected tendencies. The shape of the Ti-LMV peaks indicates that Ti in sublayer I and II is essentially oxidic bonded and with increasing nitrogen content in depth nitridic. The binding state of N at the surface and in sublayer I could not be identified due to the small N content of a few at-% and the overlapping of the N and the Ti spectrum.

B. Morphology

Figure 13: *SEM micrographs of the cross sectional fracture of the $Ti_{0.74}Al_{0.26}N$ and $Ti_{0.46}Al_{0.54}N$ film oxidized 1 h at 800 °C*

Micrographs of the cross-sectional fracture of the oxidized cubic 75/25 and 50/50 MSIP film are shown in figure 13. A cross-sectional micrograph of the hexagonal film could not be taken due to the spall-off of the film during fracturing. **As** visible from the micrographs the thickness of the oxidic overlayer is in the range of 550 nm in case of the 75/25 film and 250 nm of the 50/50. The oxidic overlayer of the Ti rich film seems to be subdivided into two sublayers, discernible at the glasslike morphology of the surface near sublayer I and the more crystalline morphology of sublayer II beneath, From the determination of the crater shape combined with the EPMA linescan analysis one can estimate the thickness of the oxidic overlayer on the hexagonal 25/7.5 film in comparison to the 75/25 one to about 500 nm.

In figure 14 SEM micrographs of the cross-sectional fracture of the oxidized 40/60 MSIP film and the 50/50 dual target MSIP film are presented. The $Ti_{0.38}Al_{0.62}N$ coating maintains its dense fibrous morphology, film adhesion to the substrate appears better than in the as-deposited state. The oxidized structure reveals no oxide overlayer of different morphology to that of the bulk. This is reasonably in accordance with the reported oxide layer thickness of less than 80 nm determined by EPMA.
Oxidation of the dual target MSIP film results in largely identical coating morphology as that

of the 50/50 MSIP coating deposited with an alloyed target, with similar oxide layer thickness of less than 500 nm. The as-deposited columnar microstructure is preserved.

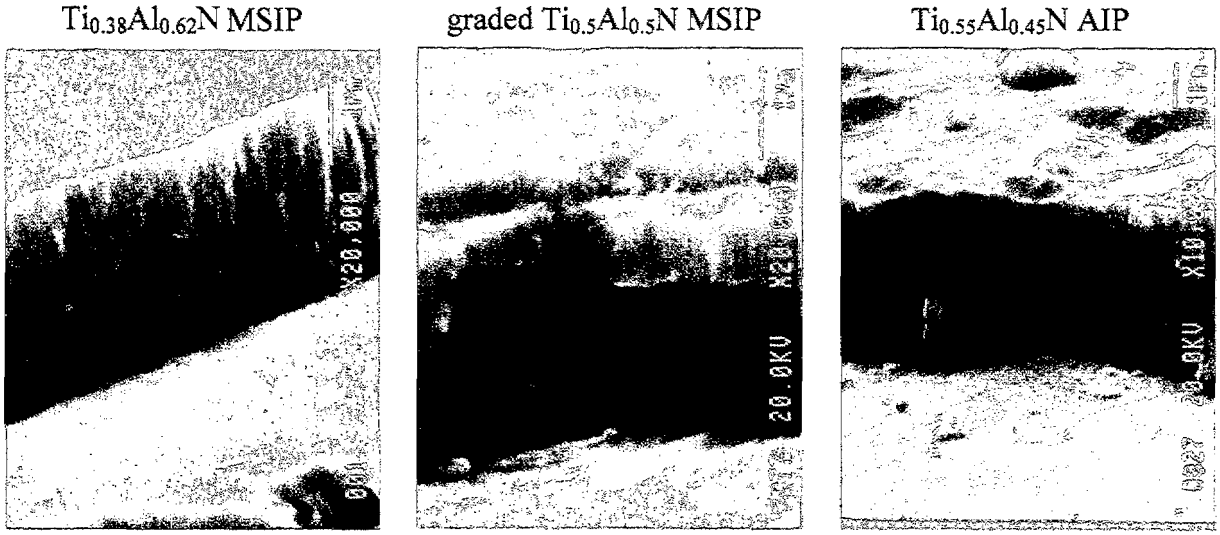

Figure 14: *SEM micrographs of the oxidized (800 °C) 40/60 MSIP, dual target 50/50 MSIP, and the 50/50 AIP film*

The cross-sectional fracture of the oxidized AIP film is also presented in figure 14. An oxide overlayer of about 500 nm is formed on the nitridic film, visible as a region of different morphology to that of the bulk. The nitridic film grain structure remains in the as-deposited columnar microstructure. No microcracking is evident. The size of the conical shaped film defects observed varies from the. submicron range up to 3 μm above the surface of the coating. The diameter of the pin holes observed in adjacent areas of the film fracture region are consistent with the size of the defects. R is likely that these pin holes are formed as a result of the conical defects becoming dislodged either during oxidation or sample preparation. The wide evidence of pin hole formation is recognized as a significant problem, where rapid diffusion and oxidation pathways are formed when any arc droplets are dislodged from the film. Structural defects with a different morphology to that of the droplets are observed. They are identified as defects which had been formed during deposition as a result of the reduced energy associated with pulsed d.c. biasing technique.

C. Structure

Figure 15 shows the diffraction patterns of the oxidized MSIP films deposited with one compound target, taken by thin film XRD. Ti in the oxidic overlayers of the $Ti_{0.74}Al_{0.26}N$, $Ti_{0.46}Al_{0.54}N$, and the $Ti_{0.25}Al_{0.75}N$ film is present in two modifications, namely anatase and rutile. Fe and β-Fe_2O_3 are peaks of the substrate. As it is not to exclude that TiO_2 is textured, evaluation of the peak intensity does not give information about the phase proportions. As no aluminum oxide can be identified, alumina has to be present in an X-ray amorphous state. The

analysis of the oxide overlayer formed at the surface of the 40/60 film does not show any oxide phase. Only one peak could be associated with rutile, so it is not definitely. Probably, the oxide overlayer mainly consists of X-ray amorphous alumina. The XRD analysis of the oxidized AIP

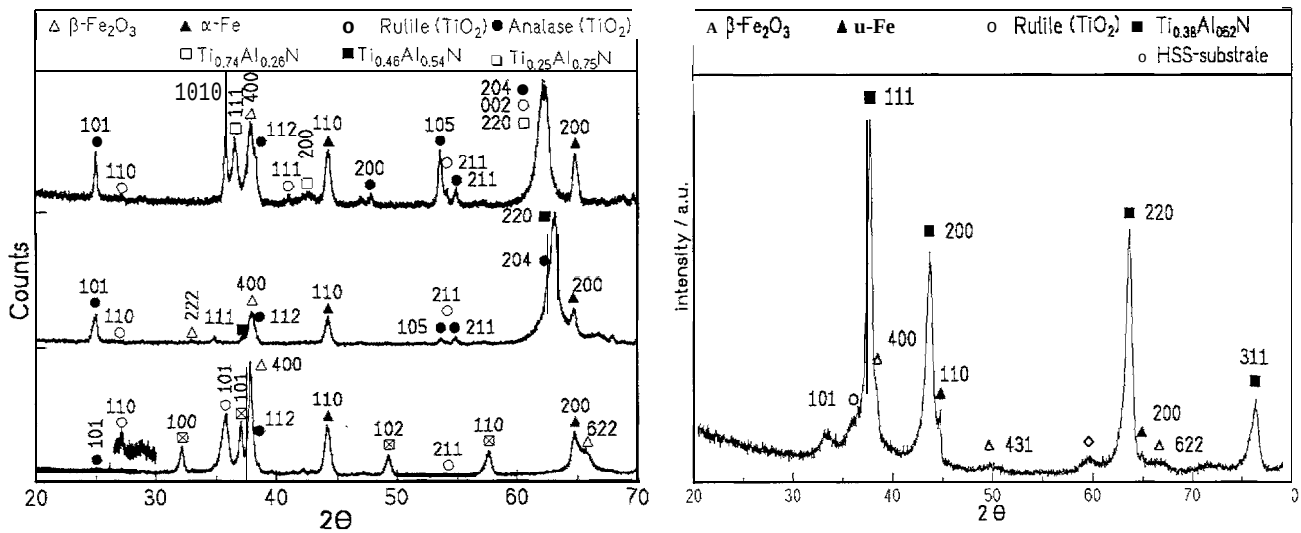

***Figure** 15: X-my diffraction patterns of the MSIP films deposited with one compound target, oxidized 1 h at 800 'C*

film leads to the same result as in case of the 50/50 MSIP film

D. Mechanical properties

Selected results of mechanical testing of the different films are shown in table 2. Generally, a decrease in microhardness is observed after oxidation of the $Ti_{1-x}Al_xN$ films 1 h at S00 'C. Only the $Ti_{0.46}Al_{0.54}N$ coating reveals a distinct increase in microhardness of more than 1000 HV0.05. The very large reduction of microhardness of the $Ti_{0.38}Al_{0.62}N$ film is surprising, this perhaps due to the very thin oxide overlayer and the failure of the nitridic film or substrate. Also measurement of the critical load, expressing adhesion of the films, shows just for the 50/50 MSIP film an increase after oxidation. The very high values of microhardness and critical load of the AIP film in the as-deposited state (and even after oxidation at 650 °C) do not remain after high temperature oxidation. The MSIP film deposited with two separate targets reveals acceptable values, but not as good as in case of the comparable homogeneous MSD? film. Nanohardness testing shows a decrease of nanohardness in case of the examined MSIP films, whereas that of the AD? film seems to increase. But as mentioned above, the values displayed a large scatter due to the roughness of the surface, caused by the droplets. Remarkable for the 40/60 MSIP film is its impact resistance. The first small cracks appeared on the oxidized films surface after 20000 impacts with a load of 900 N. Even after 50000 impacts the substrate was not to be seen. No other film investigated here has withstood so high test conditions.

4. Conclusions

Investigation of the relations between deposition processes, film compositions, and operational film properties by studies of composition, structure, morphology, binding states, and mechanical/tribological properties revealed that is is now possible to prepare $Ti_{1-x}Al_xN$ films with tailored properties concerning oxidation and wear resistance. Best high temperature oxidation resistance were detected in case of a MSIP film deposited with an insert target of a 40/60 Ti/Al ratio. For applications, where mainly mechanical stresses at lower temperature occur, an AIP film deposited in the new developed pulsed bias mode using a cathode with a 50/50 Ti/Al ratio would be most appropriate. The investigated MSIP film deposited with a powder metallurgical 50/50 target combines both properties, each of them exhibiting good, but slightly lower values of the corresponding parameters. This kind of complex testing presented in this work has shown to be appropriate for the development and optimization of such hardcoatings and processes for their preparation.

Acknowledgements

The financial support granted by the European Union under the Brite-EuRam II programme for the project "The Influence of Different Low-Temperature Vapour Deposition Techniques on the Operational Properties of Metastable Hardcoatings", contract No. BRE 2 - CT 92 - 0155, project No. BRE 2-0155, is gratefully acknowledged.

References

[1] N. Ammann, P. Karduck, Microbeam Anal. 1990, 150

[2] A. von Richthofen, D. Neuschütz, J. Anal. Chem. 1994,349, 136

[3] International Centre for Diffraction Data, 1601 Park Lane, Swarthmore, Pennsylvania 19081-2389 USA

[4] O. Knotek, M. Böhmer, T. Leyendecker, J. Vat. Sci. Technol. **1986**, A4, 2695

[5] T. Ikeda, H. Satoh, Thin Solid Films 1991, 195,99

[6] G. Håkansson, J.-E. Sundgren, D. McIntyre, J.E. Greene, W.-D. Münz, Thin Solid Films 1987, 153,55

[7] D. Münz, J. Vat. Sci. Technol. 1986, A4, 2717

[8] S. Hofmann, H. A. Jehn, Surf. Interface Anal. 19S8, 12,329

[9] H. Jehn, S. Hofmann, D. Münz, Metall 1988,42,658